RAA 2021 Vol. **21** No. **1**, 16(7pp) doi: 10.1088/1674-4527/21/1/16
© 2021 National Astronomical Observatories, CAS and IOP Publishing Ltd.
http://www.raa-journal.org *http://iopscience.iop.org/raa*

***R**esearch in*
***A**stronomy and*
***A**strophysics*

A simulation experiment on the GM estimation for Comet 133P/Elst-Pizarro

Wu-Tong Gao[1], Jian-Guo Yan ⋆[1], Wei-Tong Jin[1], Xuan Yang[1], Chen Yang[2], Mao Ye[1], Fei Li[1] and Jean-Pierre Barriot[1,3]

[1] State Key Laboratory of Information Engineering in Surveying, Mapping and Remote Sensing, Wuhan University, Wuhan 430079, China; *jgyan@whu.edu.cn*
[2] China Academy of Space Technology, Beijing 100094, China
[3] Geodesy Observatory of Tahiti, University of French Polynesia, BP 6570, 98702 Faaa, Tahiti, French Polynesia

Received 2020 April 5; accepted 2020 July 12

Abstract In China's asteroid mission to be launched around 2025, (7968) 133P/Elst-Pizarro (hereafter 133P) will be the second target, after a visit to asteroid (469219) Kamo'oalewa. This paper describes a simulation of precise orbit determination for the spacecraft around comet 133P, as well as estimation of its gravitational parameter (GM) value and the solar radiation pressure coefficient C_r for the spacecraft. Different cometocentric distances of 200, 150 and 100 km orbits are considered, as well as two tracking modes: exclusive two-way range-rate mode (Earth station to spacecraft) and combinations of two-way range-rate and local spacecraft onboard ranging to the comet. Compared to exclusive two-way range-rate, the introduction of local ranging observables improves the final GM uncertainties by up to one order of magnitude. An ephemeris error in the orbit of 133P is also considered, and we show that, to obtain a reliable estimate of the GM for 133P, this error cannot exceed a one km range.

Key words: celestial mechanics — space vehicles — comets: individual (133P/Elst-Pizarro) — methods: statistical

1 INTRODUCTION

Main belt comets are defined as main belt small bodies showing comet-like activity. 133P/Elst-Pizarro (hereafter 133P) is one of them, and has drawn people's interest since it was first observed in 1979. 133P was first identified as an asteroid based on its orbital properties (Hsieh et al. 2004), but its cometary nature was discovered in 1996 (Elst et al. 1996). 133P has a semimajor axis of 3.16 AU, an eccentricity of 0.15 and an inclination of 1.39° in the J2000 frame. It is thought to be a member of the Themis asteroid family (Toth 2000). Previous observations show that the semi-axis of 133P's nucleus is about $a \sim 2.3$ km and $b \sim 1.6$ km in the plane-of-sky (Hsieh et al. 2009).

A mission to 133P has already been considered by several space agencies (Castalia mission, Snodgrass et al. 2018; Caroline mission, Jones et al. 2018). An asteroid mission including 133P was approved in 2019 by the Chinese Authorities and its launch is planned for 2025 (China National Space Administration 2019). The objective of this mission is to explore the near-Earth asteroid (469219) Kamo'oalewa (Reddy et al. 2017), take samples from it and then execute a rendezvous with 133P around 2030.

The gravitational parameter (GM) value of an asteroid and its rotation state can be determined from the orbit perturbations of a spacecraft in sufficiently close proximity (67P/Churyumov-Gerasimenko comet, Godard et al. 2017; Bennu asteroid, Scheeres et al. 2019; Ryugu asteroid, Watanabe et al. 2019; Toutatis asteroid, Huang et al. 2013). The orbit perturbations can be measured in several ways that can be classified as measurements of relative distances and velocities, from spacecraft to Earth or spacecraft to a body. In addition, ancillary parameters such as solar radiation pressure coefficient can have an important influence for small bodies with a weak gravity field like 133P. A recent study has also proposed a method of estimating GM from line-of-sight accelerations (Jian et al. 2019).

The following describes how this paper has been arranged. In Section 2, we introduce our orbit modeling method, the force model, the characteristics of the orbit of the spacecraft and the types of observables. In

⋆ Corresponding author

Section 3, we give the results of estimations for different cometocentric distances and different tracking modes. In addition, we analyze the effect of different levels of errors on the ephemeris of 133P. In Section 4, conclusions are drawn and recommendations are made for the planning of the China's asteroid mission.

2 METHOD AND MODELS

The software for orbit determination and ancillary parameter estimation employed in this work was developed by Wuhan University (Ye et al. 2017), and uses a standard weighted, linearized least squares approach. It makes use of NAIF's SPICE library (Acton 1996) and SOFA library (Faure et al. 2012). This software has been successfully applied to several planetary cases (Moon, Ye et al. 2018; Mars, Yan et al. 2017; Mercury, Yan et al. 2019). As already mentioned, the gravitational pull of 133P is weak, so other small forces acting on the spacecraft must be modeled with precision. The orbital motion equation of the spacecraft is

$$\frac{d^2\boldsymbol{r}}{dt^2} = \boldsymbol{a}_{\rm Sun} + \boldsymbol{a}_{\rm NB} + \boldsymbol{a}_{\rm SRP} + \boldsymbol{a}_{\rm Rel} \qquad (1)$$

where $\boldsymbol{r}$ is the position vector of the spacecraft in the inertial frame. The terms in the right hand side represent central gravity of Sun, N-body perturbations, solar radiation pressure, relativistic effect, respectively. Figure 1 summarizes the magnitude of these forces with respect to the distance from 133P. We only consider the perturbation of 133P as the point-mass gravity, because in our simulation the closest distance of the spacecraft to 133P is 100 km, which makes the second degree gravity field negligible (the effect of C_{20} term to the spacecraft orbit is only serval meters, which is much less than the spacecraft orbital accuracy).

The solar radiation pressure force is the dominant non-gravitational force in our simulation. According to (Montenbruck & Gill 2000), this sun-pointing force may be expressed as:

$$\boldsymbol{a}_{\rm SRP} = -vP_{\odot}C_r{\rm AU}^2\frac{A}{m}\frac{\boldsymbol{r}_{\odot}}{|\boldsymbol{r}_{\odot}|^3} \qquad (2)$$

where v is the shadow function, $P_{\odot} = 4.56\times10^{-6}\,{\rm N\,m^{-2}}$, AU=149597870.7 km, C_r and A are the reflectivity and area of the spacecraft surface, m is the mass of the spacecraft, and $\boldsymbol{r}_{\odot}$ is the position vector from the spacecraft to Sun in the inertial frame. The unknown to be determined is C_r.

In this study, we only considered the central gravity parameter of 133P. No orientation parameters are included as the minimum distance of spacecraft to body considered is 100 km. An assumed value of GM is required for the linearized equations of motion. If we suppose that the nucleus of 133P is spherical with a radius of 2 km and density of $1300\,{\rm kg\ m^{-3}}$ (Jewitt et al. 2014), we obtain a rough estimate of $2.66972\times10^{-6}\ {\rm km^3\,s^{-2}}$. Using the assumed GM, we estimate the Hill radius of 133P to be 892 km.

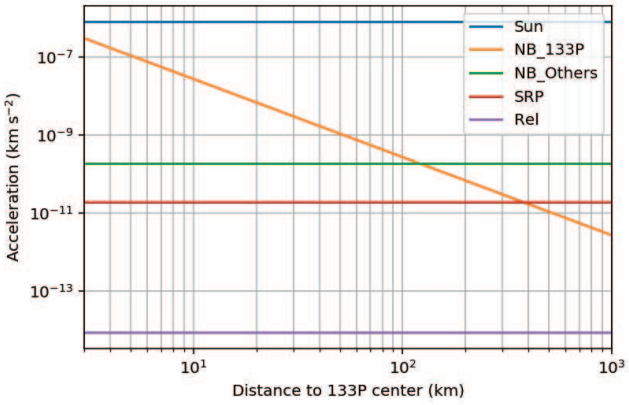

Fig. 1 Acceleration acting on the spacecraft w.r.t. distance to the center of 133P. The lines represent (1) Central gravitational of Sun labelled as Sun, (2) N-Body perturbation of 133P labelled as NB_133P, (3) N-Body perturbation of bodies other than 133P and the Sun labelled as NB_Others, (4) Solar radiation pressure labelled as SRP, and (5) Relativistic effect labelled as Rel (Gérard & Luzum 2010).

Two reference frames are used in this work. The first one is Earth mean equator and equinox of J2000 frame, which is called J2000 in SPICE. The J2000 frame is assumed to be an inertial frame and is used in the whole computation process of our software. The second one is the so-called Home Position of 133P and was introduced for the Hayabusa mission (Ikeda et al. 2003). The z direction is determined as the vector from 133P to Earth, and the y direction is defined as the cross product between the 133P-Sun vector and the 133P-Earth vector. The x direction verifies the right-hand rule. This frame is used to generate the spacecraft initial orbit.

We divided our simulation orbits into three classes: altitudes of 200, 150 and 100 km with respect to the comet center (z-component in the Home Position frame, x and y components being set to zero). The initial velocities were chosen to correspond to circular orbits with their plane normal vector perpendicular to the Earth-133P direction. The acceleration of the target body at the above altitudes is about $10^{-13}\,{\rm km\ s^{-2}}$. This is in the same order of magnitude as the preliminary orbits for the Hayabusa mission to asteroid Itokawa (Ikeda et al. 2003) and for the Rosetta mission to comet 67P/Churyumov-Gerasimenko (Pätzold et al. 2016). The main reason for choosing altitudes of this order of magnitude was to avoid any outgassed debris floating free around these bodies.

For each case, a 9-day orbit using the initial state is generated and divided it into three equal arcs of 0–3 days, 3–6 days, and 6-9 days, and the initial states for each arc are estimated. The global solve-for parameters were GM and C_r for these arcs (multi-arc strategy of Alessi et al. 2012).

Two types of observables were used. The first type is a classical two-way range-rate observable between the Earth and the spacecraft (Moyer 2000). The second one is a generic onboard ranging observable (for example, using stereo-photogrammetry, laser ranging, or radar ranging) from the spacecraft to the body. They are illustrated in Figure 2. As we are ignoring the shape of the body in this simulation, we assume that this generic distance measurement is the distance between the gravity center of the body and the spacecraft's gravity center. The simulated observables are generated by adding Gaussian distribution noise to the computed values. The standard deviation of the noise in the two-way range-rate is assumed to be $0.1\ \mathrm{mm\,s^{-1}}$ with an interval of 60 s. For the onboard ranging observable, we take instantaneous measurements separated by 60 s and use a noise level of 10 m. A full description of the force models and the observables is provided in Table 1.

3 RESULTS

We first evaluated the relative contribution of our two types of observables to the estimation of GM. We have to stress at this stage that the onboard ranging observables cannot be used alone, as they only contain the dynamics of other Solar system bodies as second-order quantities (tidal accelerations). To address this, we computed a reference orbit at a 100 km altitude using the assumed GM of 133P given in Section 2. Thereafter, perturbed orbits were integrated, with the same initial vector and C_r coefficient by adding a 1%, 0.1%, or 0.01% relative bias to the assumed GM. The results of calculating residuals of observables between the perturbed orbits and the reference orbit are shown in Figure 3.

The result in Figure 3 shows the sensitivity of these two observables to the GM in a 100 km orbit in 9 days. We can have an understanding of how large the GM error can be sensed in these two observables. By comparing the orange areas of Figure 3, we can see that, for the onboard ranging data, the 0.1% GM error can cause a maximum error about 70 m, which is significantly larger than its noise (10 m). While for the two-way range-rate data, the maximum error is about 0.2 mm s^{-1} with the 0.1% GM error, which is hard to distinguish from the corresponding noise ($0.1\ \mathrm{mm\,s^{-1}}$). Generally speaking, Figure 3 clearly indicates that the inclusion of onboard ranging is crucial for an estimation of GM under the error of 0.1%.

In a second step, we carried out modeling of the GM and C_r coefficient for three different comet distances: 100, 150 and 200 km. For each altitude, we considered three arcs of 3 days, with determination of the initial vectors of each arc. In our simulation, we used two tracking modes. They are (I) two-way range-rate only and (II) two-way range-rate plus onboard ranging. The results are shown in Figure 4.

We estimated local parameters (i.e. the initial state vector of each arc) for each case, and the 1σ uncertainties in initial position are shown in Figure 4. Their final 1σ uncertainties range from 20 m to 200 m. Under the same observation conditions, an orbit close to 133P can reduce the formal uncertainties in position. This happens because the stronger gravitational attraction of 133P maps to higher velocities with respect to the body and allows greater observability of the spacecrafts initial state vector. With respect to the 200 km orbit, the formal position uncertainties in the 150 km orbit improve by 40% and 112% for tracking mode (I) and (II), respectively. With respect to the 150 km orbit, the uncertainties in the 100 km orbit improve by 109% and 228%, respectively. If tracking mode (II) is used, the formal uncertainties improve by 160%, 326%, and 602% compared to tracking mode (I) for the 200, 150 and 100 km orbit, respectively. In addition, we computed the true error, which is defined as the difference between the solved and the initial reference position components. The formal uncertainty is a statistical result and should agree with the true error because the same force model was used in the construction of pseudo-observables and in the least-squares inversion. The true errors in position components for each case are almost consistent with their formal uncertainties, with an average true-to-formal ratio of about 0.86. The result of GM estimations are presented in Figure 5 and Table 2.

Figure 5 gives the relative GM formal uncertainties over 9 days. Table 2 shows the true error in the final estimated GM. From Figure 5, we can see that in tracking mode (I), the final 1σ uncertainty is about 0.159% of the assumed GM value for an orbital height of 200 km, and that there is no apparent decrease when lower orbits are used (uncertainties of 0.199% and 0.196% for orbital height of 150 km and 100 km, respectively). While in tracking mode (II), the lower-altitude orbit produces a much better GM result than the higher-altitude orbit. The uncertainty decreases from 0.031% to 0.008% with a decrease in orbital height from 200 km to 100 km. The improvement can be also seen in the final relative true errors presented in Table 2. Compared to the results for using tracking mode (I), tracking mode (II) improves the uncertainties in GM estimation by about 4, 10, and 23 times for the 200, 150 and 100 km cases, respectively. The true-to-formal ratio of

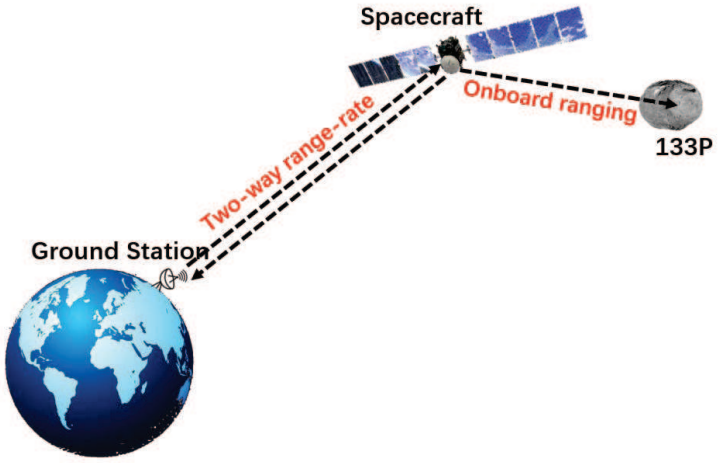

Fig. 2 Illustration of the two types of observable used in our simulation.

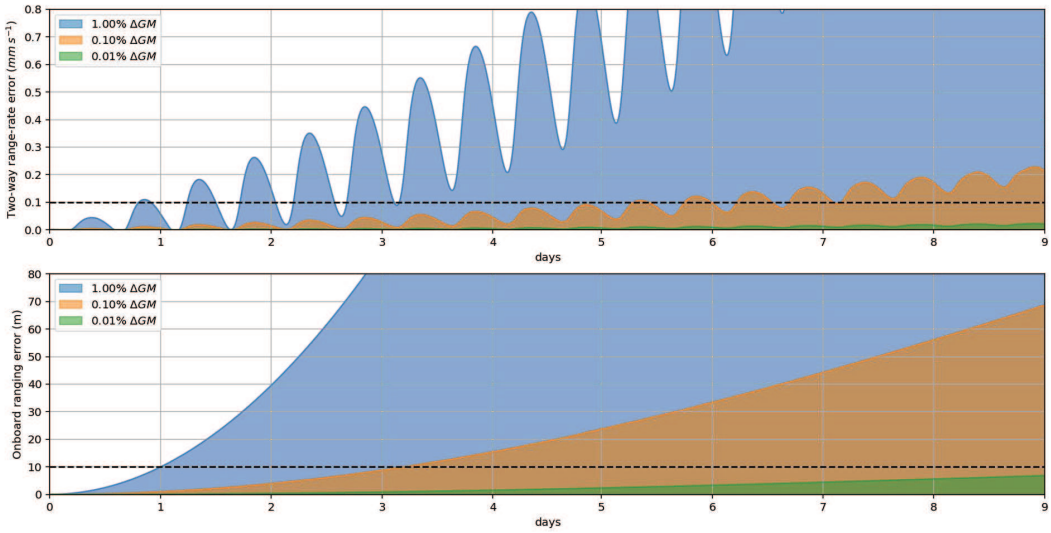

Fig. 3 Evolution of observable errors over 9 days, between the GM-perturbed orbits and the 100 km reference orbit for the two kinds of observable: range-rate (*top*) and onboard ranging (*bottom*). The black dotted lines in each sub-plot are the respective noise levels of the observables. Onboard ranging is more sensitive to GM-perturbations with respect to range-rate from the Earth by nearly one order of magnitude.

Table 1 Details of the Force Models and Observables Used in Our Simulation

Model	Description
Force models	Central gravitational of Sun, from JPL ephemeris DE431 (Folkner et al. 2014).
	Perturbations of 133P, all planetary bodies in solar system, Ceres, Vesta, and Pallas from DE431 and JPL Small-Body Database (Jet Propulsion Laboratory 2016).
	Cannonball model of solar radiation pressure, mass to area ratio 50 $\mathrm{kg\ m^{-2}}$ and C_r=1.5 (Montenbruck & Gill 2000).
	Relativistic effect of Sun (Gérard & Luzum 2010).
Observable models	Two-way range-rate, interval of 60 s, noise level of $0.1\mathrm{mm\ s^{-1}}$
	Onboard ranging to 133P, 60 s, noise level of 10 m
	Earth tracking station: Kashi station and JMS station
	Uplink frequency: 7168883696.0 Hz
	Transponder ratio: 880/749
	Cutoff angle: 10°

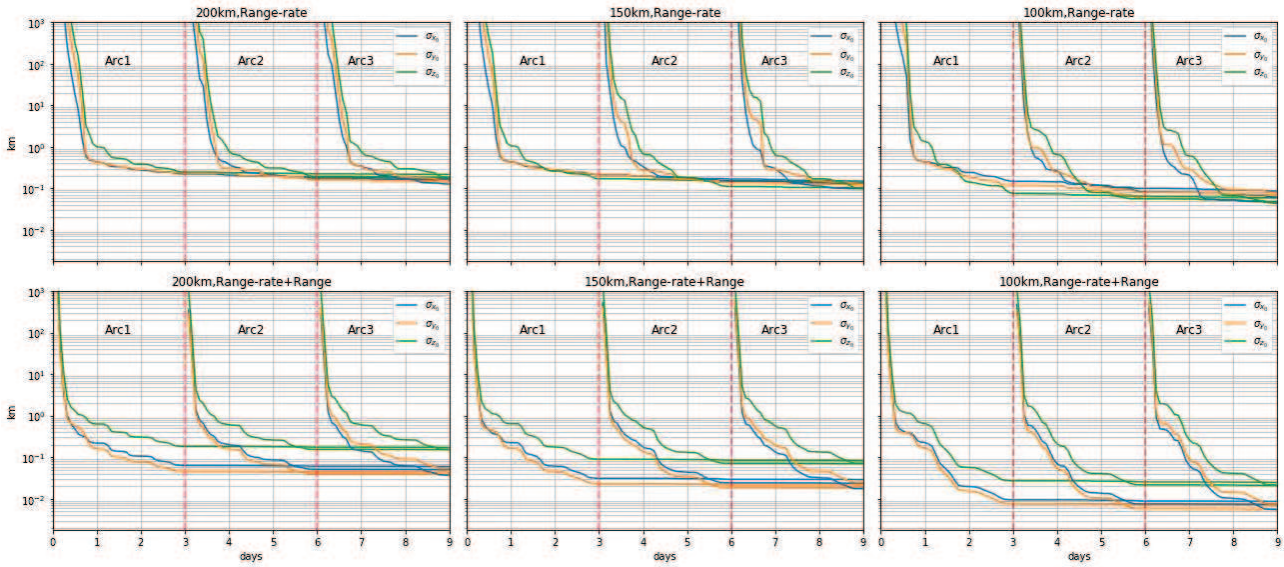

Fig. 4 1σ uncertainty in spacecraft initial positions w.r.t. observation time in 200 km (*left columns*), 150 km (*middle columns*) and 100 km (*right columns*) orbits using tracking modes of (I) two-way range-rate only (*top row*) and (II) two-way range-rate + onboard ranging (*bottom row*).

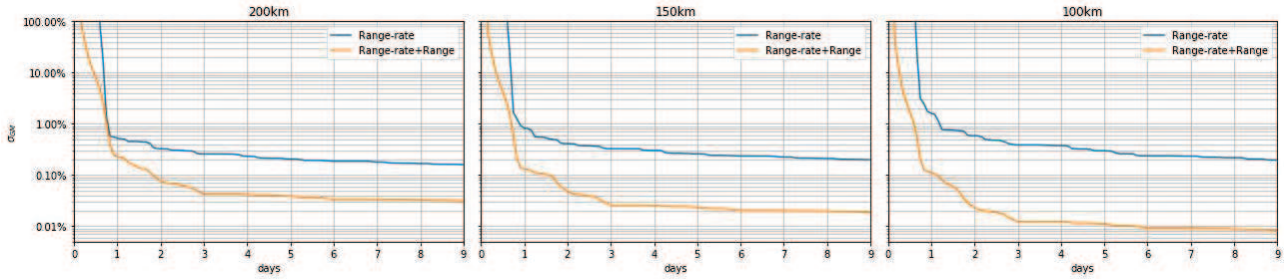

Fig. 5 Relative 1σ uncertainties in 133P GM estimation w.r.t. observation time, for 200 km (*left column*), 150 km (*middle column*), 100 km (*right columns*) orbits using tracking modes of (I) two-way range-rate only (blue lines) and (II) two-way range-rate + onboard ranging (*orange lines*).

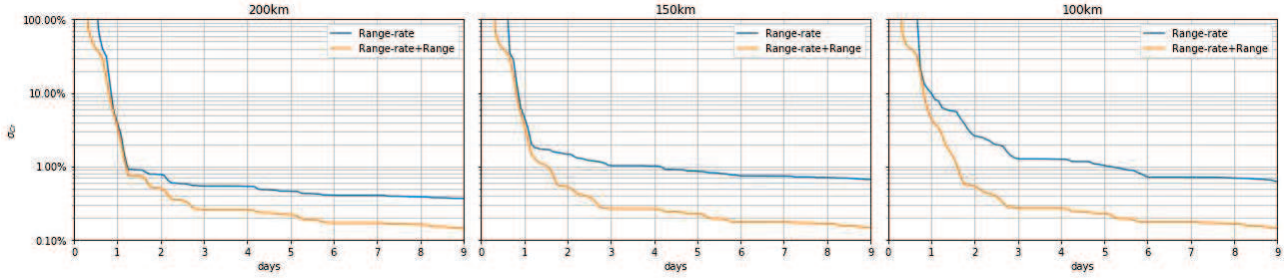

Fig. 6 Relative 1σ uncertainty for estimated C_r w.r.t. observation time, 200 km (*left column*), 150 km (*middle column*), 100 km (*right column*) orbits using tracking modes of (I) two-way range-rate only (*blue lines*) and (II) two-way range-rate + onboard ranging (*orange lines*).

Table 2 Final Relative True Error of 133P's GM over 9 Days Observation

	Tracking mode	200 km orbit	150 km orbit	100 km orbit
(I)	two-way range-rate only	0.145%	0.247%	0.055%
(II)	two-way range-rate + onboard ranging	0.111%	0.086%	0.014%

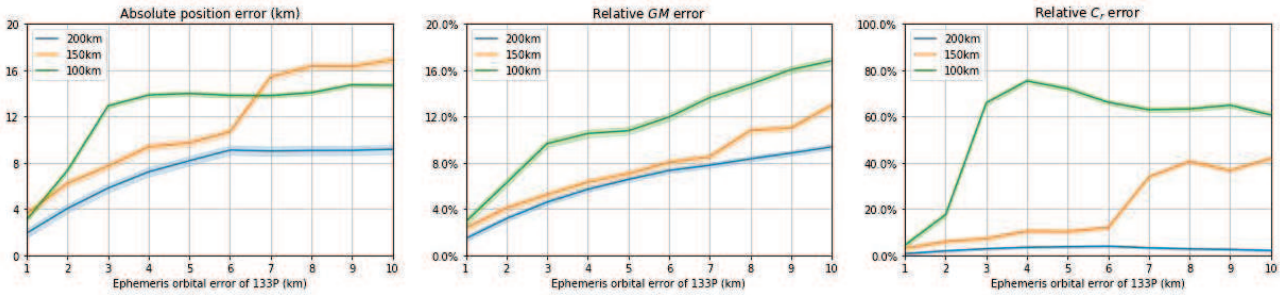

Fig. 7 True errors in initial position, GM and C_r and their corresponding 1σ uncertainties (*shaded areas*) in 200, 150 and 100 km orbits, by including an ephemeris error ranging from 1 km to 10 km.

Table 3 Final Relative True Error of C_r over 9 Days Observations

	Tracking mode	200 km orbit	150 km orbit	100 km orbit
(I)	two-way range-rate only	0.222%	1.352%	0.717%
(II)	two-way range-rate + onboard ranging	0.348%	0.487%	0.172%

the final GM is from 0.07 to 1.23 in these cases, which means that the deviations in GM results are all less than their corresponding 3σ uncertainties.

In our computation, we consider the influence of solar radiation because the magnitude of this perturbation force is close to that of 133P's gravitational force, and the modeling of solar radiation pressure will affect solution of 133P's GM. The relative 1σ uncertainties and true errors in the estimated radiation pressure coefficient are shown in Figure 6 and Table 3.

As Figure 6 shows, there is an increase in both the uncertainties and the true errors in C_r in the lower orbits compared to the higher orbits. This is probably because the gravitational of 133P tends to dominate the acceleration on the spacecraft in the lower orbits, and makes the solar radiation pressure less apparent in the observables. Similar to the GM estimation results, tracking mode (II) improves the C_r uncertainties by 2, 3, and 3 times compared to tracking mode (I) for the 200, 150 and 100 km orbits, respectively. The final true-to-formal ratios of C_r in these cases range from 0.28 to 2.05 and the a posteriori residuals of observables also follow a Gaussian distribution. The 133P ephemeris is also a prerequisite in orbit determination and parameter estimation. In the above computation, it is assumed that there is no systematic error in the ephemeris of 133P. However, there is of course an uncertainty in the 133P ephemeris, mainly along its orbit. We can simulate this error by adding a time bias to the ephemeris. A time error of 0.05 s in the ephemeris of 133P from the JPL small body database causes a position error of about 1 km. By adding a time error from 0.05 s to 0.5 s with a step of 0.05 s, we produced a list of perturbed ephemerides with a position error ranging from 1 km to 10 km. We set the a priori errors as 10 km for the initial position and 100 % with respect to their assumed value for the GM and C_r estimates. Tracking mode (I) fails to achieve convergent results for the three different orbital altitudes. The errors in initial position, GM and C_r with respect to different ephemeris errors using tracking mode (II) are shown in Figure 7.

The 133P's systematic ephemeris error affects more GM and C_r estimates for low altitude orbits, with position determination errors larger than the corresponding ephemeris error. The absolute true-to-formal ratios for the GM estimates are large (6–39, 7–44 and 8-50 for 200, 150, 100 km orbit, respectively). This is similar to a previous simulation that was performed for the case of asteroid Kamo'oalewa (Jin et al. 2020), in which the true-to-formal ratio of the GM estimation was about 20 after introducing comparable ephemeris errors. An ephemeris error of more than 4 km in a 100 km altitude orbit produces a significantly misleading C_r estimate (with a relative error of more than 60%). This shows that the ephemeris error is a critical point.

4 CONCLUSIONS

We can draw the following conclusions from our simulation. Firstly, by reducing the altitude of spacecraft orbit we obtain better spacecraft initial state and GM estimates, but worse C_r estimates. Secondly, introducing onboard ranging to 133P can significantly improve the result of orbit determination, as well as the estimation of GM and C_r. The closer the orbit to 133P, the greater the improvement. Finally, the impact of the ephemeris error for 133P is not negligible. For the 100 km altitude orbit solution, a 4 km ephemeris error for 133P produces a 14 km initial position error, a 10% GM error and 75% C_r error.

In the force model for 133P, only point-mass gravitational force is considered. For the further investigation of a closer orbit to 133P, a detailed, high degree and order gravitational force model would be included. The onboard camera could model the shape of 133P at a close distance, which would help to improve spacecraft orbit determination. In addition, in China's 2025 asteroid mission, it would be possible to put a transponder on the 133P surface to carry out range-rate measurement using an Earth station-spacecraft-transponder link. Combining data from these tracking modes with Earth station range-rate tracking data and image data will enable gravity field and rotational dynamics estimations to be carried out with higher resolution, including a possible modeling of rotation-rate and precession. A highly precise ephemeris of 133P is also a requirement. This ephemeris error estimation can be conducted as a by-product of the GM estimation, as the relative positioning of the spacecraft with respect to the gravity center of 133P gives an indirect constraint to the ephemeris error (Konopliv et al. 2002).

Acknowledgements This work is supported by the National Natural Science Foundation of China (U1831132 and 41874010) and Innovation Group of Natural Fund of Hubei Province (2018CFA087); Jean-Pierre Barriot is supported by a DAR fund in planetology from the French Space Agency (CNES).

References

Acton, C. H. 1996, Planet. Space Sci., 44, 65
Alessi, E. M., Cicalò, S., Milani, A., & Tommei, G. 2012, MNRAS, 423, 2270
China National Space Administration. 2019, Announcement of Opportunities for Scientific Payloads and Projects onboard Asteroid Exploration Mission
Elst, E. W., Pizarro, O., Pollas, C., et al. 1996, IAU Circ., 6456, 1
Faure, F., Duriez, C., Delingette, H., et al. 2012, in Soft Tissue Biomechanical Modeling for Computer Assisted Surgery (Springer), 283
Folkner, W. M., Williams, J. G., Boggs, D. H., et al. 2014, Interplanetary Network Progress Report, 196, 42
Gérard, P., & Luzum, B. 2010, Bureau International Des Poids Et Mesures Sevres (France), 1
Godard, B., Budnik, F., Bellei, G., Muñoz, P., & Morley, T. 2017, Issfd-2017, 16
Hsieh, H. H., Jewitt, D. C., & Fernández, Y. R. 2004, AJ, 127, 2997
Hsieh, H. H., Jewitt, D., & Fernández, Y. R. 2009, ApJL, 694, L111
Huang, J., Ji, J., Ye, P., et al. 2013, Scientific Reports, 3, 3411
Ikeda, H., Kominato, T., Matsuoka, M., Ohnishi, T., & Yoshikawa, M. 2003, AIAA 57th International Astronautical Congress, IAC 2006, 7, 4430
Jet Propulsion Laboratory. 2016, JPL Small-Body Database Browser
Jewitt, D., Ishiguro, M., Weaver, H., et al. 2014, AJ, 147, 117
Jian, N.-C., Yan, J.-G., Ping, J.-S., Barriot, J.-P., & Rodriguez, J. A. P. 2019, RAA (Research in Astronomy and Astrophysics), 19, 048
Jin, W. T., Li, F., Yan, J. G., et al. 2020, MNRAS, 493, 4012
Jones, G. H., Agarwal, J., Bowles, N., et al. 2018, Advances in Space Research, 62, 1921
Konopliv, A. S., Miller, J. K., Owen, W. M., et al. 2002, Icarus, 160, 289
Montenbruck, O., & Gill, E. 2000, Satellite Orbits: Models, Methods and Applications, 134 (Springer-Verlag Berlin Heidelberg), 220
Moyer, T. D. 2000, Deep Space Communications and Navigation Series, 2, 549
Pätzold, M., Andert, T., Hahn, M., et al. 2016, Nature, 530, 63
Reddy, V., Kuhn, O., Thirouin, A., et al. 2017, in AAS/Division for Planetary Sciences Meeting Abstracts #49, 204.07
Scheeres, D. J., McMahon, J. W., French, A. S., et al. 2019, Nature Astronomy, 3, 352
Snodgrass, C., Jones, G. H., Boehnhardt, H., et al. 2018, Advances in Space Research, 62, 1947
Toth, I. 2000, A&A, 360, 375
Watanabe, S., Hirabayashi, M., Hirata, N., et al. 2019, Science, 364, 268
Yan, J., Liu, S., Yang, X., et al. 2019, Ap&SS, 364, 58
Yan, J., Yang, X., Ye, M., et al. 2017, Ap&SS, 362, 123
Ye, M., Li, F., Yan, J., et al. 2017, Acta Geodaetica et Cartographica Sinica, 46, 288
Ye, M., Li, F., Yan, J., et al. 2018, Ap&SS, 363, 236